ELSEVIER

Chemical Engineering Journal 92 (2003) 41–54

Chemical Engineering Journal

www.elsevier.com/locate/cej

Analysis of operating variables on the performance of a reactor for total hydrogenation of olefins in a C_3–C_4 stream

S.P. Bressa [a,b], J.A. Alves [a,b], N.J. Mariani [a,c], O.M. Martínez [a,b], G.F. Barreto [a,b,*]

[a] *Departamento de Ingeniería Química, Facultad de Ingeniería, Universidad Nacional de La Plata, La Plata, Argentina*
[b] *Centro de Investigación y Desarrollo en Procesos Catalíticos (CINDECA), CONICET-Universidad Nacional de La Plata, Calle 47 no. 257, CC 59, CP: B1900AJK, La Plata, Argentina*
[c] *Pinmate, Departamento de Industrias, Facultad de Ciencias Exactas y Naturales, Universidad de Buenos Aires, Ciudad Universitaria, Buenos Aires, Argentina*

Received 30 October 2001; accepted 11 May 2002

Abstract

The effect of process and operating variables in the catalytic hydrogenation of unsaturate traces in C_3–C_4 streams, intended for aerosol propellant use, has been analysed. The results from catalytic tests carried out on a commercial Pd/Al_2O_3 catalyst have been used to estimate the kinetic parameters of rate expressions. The set of rate expressions is used in a mathematical model of a three-phase fixed-bed catalytic unit operated in up-flow mode. The mathematical model allowed studying the effect that variables such as temperature, pressure, hydrogen mass flow and feed composition will exert on the reactor performance.

The volatility of the hydrocarbon mixture is found to be a paramount factor in the process, as H_2 becomes diluted in the vapour phase and, consequently, the amount of H_2 dissolved in the liquid stream and the hydrogenation rates decrease significantly.

A temperature rise turned out to be detrimental for the reactor performance, as the increased hydrocarbon volatility overcomes the effect on the kinetic coefficients. This conclusion precludes the usual operating practice of rising temperature to compensate for catalytic activity decay. Instead, increasing the H_2 input and/or the operating pressure were shown to be effective alternatives for this purpose.

Keywords: Hydrogenation; Three-phase reactor; Olefins and di-olefins; Pd catalyst

1. Introduction

Because of regulations protecting the atmospheric ozone layer, propane and butane mixtures are currently employed as aerosol propellants substituting chlorofluorocarbons in spray cans. The available refinery cuts containing saturated C_3 and C_4 hydrocarbons frequently contain olefins and di-olefins, which have to be removed to obtain a product of commercial value. As conventional separation processes are not practical to bring the content of unsaturated compounds within the low specification limits (some tens of ppm), catalytic hydrogenation represents a convenient alternative.

The catalytic hydrogenation can be carried out on Pd supported catalysts, similar to those employed for selective hydrogenation processes [1]. This type of catalysts is appropriate for operation at low temperature (a tentative range may be 303–333 K) and pressures high enough to maintain the hydrocarbon stream in liquid phase and to allow a suitable H_2 partial pressure (around 1 MPa). The liquid phase operation is advantageous to reduce pressure drop through the bed and also to wash high molecular weight species, which otherwise grow up on the catalyst surface and then accelerate the loss of its activity [2].

The aim of this contribution is to analyse the effect of the main operating variables, such as temperature, pressure, hydrogen to hydrocarbon input ratio, composition of the unsaturated pool, on the performance of this kind of hydrogenation units, namely three-phase fixed-bed reactors. The range of variables was subjected to suggested bounds for operating available commercial catalysts and to typical composition of C_3–C_4 refinery streams.

In order to fulfil this objective, kinetic information and a mathematical model describing the behaviour of a fixed-bed catalytic reactor are needed.

Catalytic tests for the evaluation of reaction rate parameters have been carried out on a commercial catalyst, and will be also described here.

* Corresponding author. Tel.: +54-221-4211353; fax: +54-221-4254277.
E-mail address: barreto@dalton.quimica.unlp.edu.ar (G.F. Barreto).

1385-8947/02/$ – see front matter
PII: S1385-8947(02)00116-X

Nomenclature

a_v	interfacial area per unit bed volume (m^2/m^3)
A_f	bed section (m^2)
c_P	molar heat capacity (J/mol K)
C	concentration (mol/m^3)
$\mathbb{C}_P$	total heat capacity (Eq. (12)) (J/s K)
d_h	equivalent particle diameter ($= \varepsilon_L d_{ps}/[1.5(1-\varepsilon_L)]$) (m)
d_{pe}	equivalent particle diameter ($= V_p/6S_p$) (m)
d_{ps}	diameter of a sphere with the same surface area of the packing piece (m)
d_T	bed diameter (m)
D	diffusion coefficient (m^2/s)
D_{ax}	axial dispersion coefficient (m^2/s)
E	activation energy (J/mol)
F	total molar flow (mol/s)
F_{H_2}(st)	stoichiometric value of F_{H_2} (mol/s)
g	gravitational acceleration (m/s^2)
k	kinetic constant ($mol/s\,kg_{cat}$)
k^L	vapour–liquid (on the liquid side) mass transfer coefficient for low flux (m/s)
k^S	liquid–solid mass transfer coefficient for low flux (m/s)
k^V	vapour–liquid (on the vapour side) mass transfer coefficient for low flux (m/s)
K	vapour–liquid equilibrium constant
K^e	chemical equilibrium constant
L	liquid molar flow (mol/s)
M_{cat}	catalyst mass (kg)
MW	molecular weight (kg/mol)
n_j	moles of species j in experimental batch
N	molar flux ($mol/s\,m^2$)
P	pressure (MPa)
P_s	static pressure per reactor length (Pa/m)
Pe_L	Peclet number ($= u_L d_{pe}/D_{ax}$)
Pe'_L	modified Peclet number ($= Pe_L(Z_L/d_{pe})$)
Q_r	total heat of formation (Eq. (12)) (J/s)
Q_V	total heat of vaporisation (Eq. (12)) (J/s)
r	reaction rate ($mol/s\,kg_{cat}$)
Re	Reynolds number ($= ud_{pe}\rho/\mu$)
Sc	Schmidt number ($= \mu/\rho D$)
t	time (s)
T	temperature (K)
u	superficial velocity (m/s)
V	vapour molar flow (mol/s)
x	molar fraction in liquid phase
y	molar fraction in vapour phase
z	total molar fraction
Z	axial coordinate (m)
Z_L	reactor length (m)

Greek letters

α	stoichiometric coefficient
ΔH_k	heat of formation of species k (J/mol)
ΔP_b	frictional pressure drop per reactor length (Pa/m)
ε	bed porosity (m^3/m^3)
ε_L	liquid hold-up (m^3/m^3)
κ_{ad}	adsorption equilibrium constant
λ	enthalpy of evaporation (J/mol)
μ	viscosity (kg/m s)
ρ	density (kg/m^3)
ρ_b	catalyst mass per unit bed volume (kg/m^3)
σ	surface tension (N/m)

Subscripts and superscripts

e	exit value
H_2	hydrogen
HC	hydrocarbon
i	interphase
j, k	species j, k
L	liquid phase
LS	liquid–solid
NC	number of compounds
0	inlet conditions
S	catalyst surface
T	total
un	total unsaturates
V	vapour phase
VL	vapour–liquid

The kinetic expressions thus obtained will be used in the mathematical model of a concurrent up-flow reactor. The up-flow operation has been shown [3] to be suitable for selective hydrogenation of olefin-rich C_4 cuts. Also, it is employed for other hydrotreating processes [4,5], in particular when partial vaporisation of the liquid stream takes place [6], as it is expected to be the case in the studied application.

2. Kinetic expressions: experiments and regression

A kinetic study employing a commercial catalyst was undertaken. As summarised later on, intra-particle effects were not discriminated. Therefore, *effective* kinetic expressions were developed from a regression analysis. It was checked that the experimental conditions led to negligible external effects; so, those expressions could be directly employed in the mathematical model of an industrial unit.

2.1. Catalyst and other materials

Experiments were performed on a commercial 3-lobe catalyst with Pd at 0.45% (w/w) impregnated on a thin external layer ("egg-shell"). The pellets were 4 mm long and

the diameter of the lobes was around 1 mm. The specific volume was 0.5×10^{-3} m^3/kg.

H_2 (99.999%) and N_2 (99.999%) were purified from water and oxygen by passing the streams through a guard bed of the same catalyst followed by a 4 Å molecular sieve bed and an oxygen trap. Hydrocarbons employed were 1-butene (99.0%), *n*-hexane (HPLC 97%) and a refinery sample that were contacted with a 4 Å molecular sieve bed before use.

2.2. Experimental set-up and operation

Batch type experiments with respect to the hydrocarbon mixtures were planned because of simplicity, economy and the amount of information provided by each run.

The main components of the experimental set-up adopted for the kinetic study are sketched in Fig. 1. This reactor configuration was chosen by comparison with some other alternatives [7]. The 100 ml stirred vessel is part of a commercially available system for reaction tests. This vessel contains most of the liquid mixture in the loop. *n*-Hexane is employed as an inert solvent to facilitate the loading of the reactants and the manipulation of the samples for chromatographic analysis. The operating pressure P is maintained by feeding H_2 through a pressure regulator. The level of H_2 partial pressure, P_{H_2}, can be chosen within a wide range (from about 0.03 MPa) and maintained essentially constant during the run.

The catalyst sample is placed in an external stainless steel 1/4 in. tube with a jacket in which water at the same temperature of the stirred vessel is circulated. Catalyst samples are in the range 0.3–0.4 g. The original pellets are axially cut into three pieces. As the height of the pieces (≈1.3 mm) is still much larger than the thickness of the external active layer (of the order of 0.1 mm), any effect of internal transport limitations is preserved.

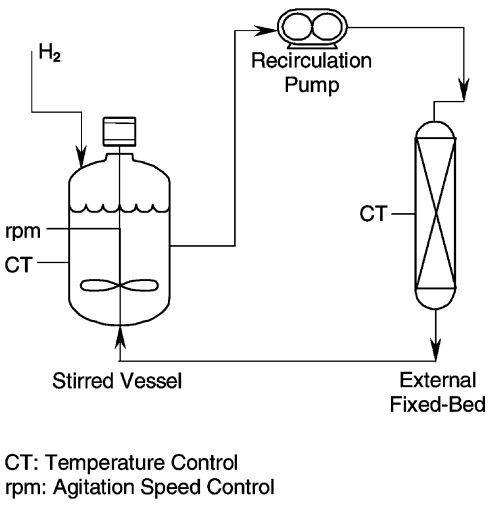

Fig. 1. Sketch of experimental set-up.

The gear micro-pump (Fig. 1) recirculates the liquid at 3.45×10^{-6} m^3/s. The recirculating liquid mixture flows downward through the catalyst bed. Temperature in the stirred vessel is controlled through an electrical heater around the vessel.

Liquid samples were analysed by gas chromatography employing a 2 m × 2 mm column packed with 0.19% picric acid on 80–100 mesh Graphpac. The separation of propane, propene, 1,3-butadiene, 1-butene, *cis*-2-butene, *trans*-2-butene and *n*-butane is achieved at ambient temperature.

Further characteristics of the experimental set-up are explained in [7].

2.3. Catalyst treatment

The catalyst samples were treated (for reduction finishing) in situ by employing a mixture of N_2 (78%) and H_2 (22%) at 327 K for a duration of 9 h. Preliminary tests showed that if in the course of the kinetic experiments the catalyst sample gets into contact with moisture, its catalytic activity drops significantly. Hence, due precautions were taken to eliminate humidity or O_2 (which produces H_2O in presence of H_2) in the gases and hydrocarbons employed for the experimental runs.

2.4. Experimental conditions

Two types of reacting mixtures were employed for the experiments:

(a) A sample from a C_3–C_4 refinery stream consisting of propene (0.64 mol%), 1,3-butadiene (0.28%), 1-butene (0.62%) and isobutane (98.46%) diluted in *n*-hexane. Operating conditions were: $T = 313$ K, $P = 0.6$ MPa and $P_{H_2} = 0.275$ MPa.

(b) A laboratory mixture of 1-butene in *n*-hexane. 1-Butene concentration (mol%) was varied from 0.78 to 4.22%. Three temperature levels between 303 and 323 K and two P_{H_2} levels (0.155 and 0.275 MPa) were studied.

2.5. Analysis of experimental data

The set of overall reactions displayed in Fig. 2 was found suitable to represent the experimental results. The *cis*-2-butene and *trans*-2-butene were not present in the reacting mixture, but they were formed either from hydrogenation of 1,3-butadiene (reactions 3 and 4) or by isomerization of 1-butene (reactions 8 and 9). Hydrogenation reactions of both 2-butenes are relatively slow and that of *trans*-2-butene turned out to be the slowest reaction. Therefore, it is important to quantify both, their rate of formation and their hydrogenation rate. The second type of reacting mixture described in Section 2.4 was mainly intended to this end.

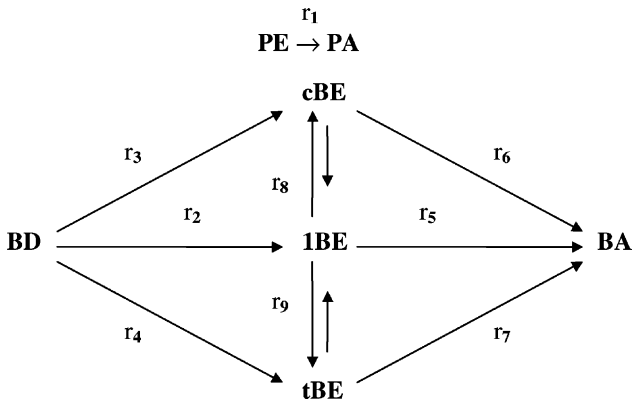

Fig. 2. Reaction network.

The set of rate expressions displayed in Table 2 has been employed to fit the results from the experimental tests. The type of dependency on mole fractions is based on analogous rate expressions proposed in literature for selective hydrogenation of C_4 cuts [2,3,8]. However, only the essential features compatible with the observed trends have been retained in this case, as the objective of the present kinetic study was to obtain a consistent description of the overall kinetic behaviour, rather than identifying an intrinsic mechanism. The following features are worth mentioning:

- Hydrogenation reactions behave irreversibly, while 1-butene isomerization reactions (reactions 8 and 9) are more accurately treated as being reversible.
- The driving term of all kinetic expressions is first order respect to the unsaturated species being consumed.
- The hydrogenation reactions showed a first order dependence on H_2 concentration, while the isomerization reaction showed a very weak dependence, which in practical terms was assumed to be nil.
- A significant inhibition effect is exerted by the unsaturates on the hydrogenation reactions, but a negligible effect was found on the isomerization reactions. Although it is very well known that the different species show large differences in adsorption strength [8], discrimination was not possible from the present data. A wider experimental range of composition and due attention to intra-particle effects would be needed to that end. For the present data, an unsaturate lump was suitable to represent inhibition effects on hydrogenation reactions.

The available information for each experimental run is the liquid composition (expressed in term of mole fraction x_j for each unsaturated species j) at a set of reaction times. As the catalytic bed operates under essentially uniform bulk liquid conditions (due to high recirculation flow), the conservation equations employed for the unsaturated species during each run were

$$\frac{dn_j}{dt} = M_{cat} r_j \quad (1)$$

where r_j is the observed rate of chemical production of species j per unit mass of catalyst sample M_{cat}. Eq. (1) can be numerically integrated with a code for solving ordinary first order differential equations.

The regression analysis to evaluate the best estimates of the effective kinetic parameters has been performed by the pack of routines GREGPACK [9] employing the multiresponse mode. Integration of Eq. (1) has been performed by the routine DDASAC included in GREGPACK.

The hydrogen molar fraction x_{H_2} was evaluated from the known H_2 partial pressure assuming equilibrium between vapour and liquid phases. The Soave–Redlich–Kwong EOS with MHSV mixing rules [10] and modified UNIFAC parameters [11] was employed to this end.

It was verified that the mass transfer resistance in liquid phase between the bulk and the solid surface was negligible [12].

The best estimates of kinetic parameters are displayed in Table 1. The effective rate constants and the lumped adsorption constant κ_{ad} correspond to $T = 313$ K. Apparent activation energies of the reactions involving *n*-butenes as reactive species (reactions 5–9) are also given. There were no data available to estimate the activation energy of propene and 1,3-butadiene hydrogenation reactions (reactions 1–4). For simulating purposes they were assumed equal to the value of 1-butene hydrogenation E_5. The temperature dependence of κ_{ad} could not be statistically inferred, so it was assumed constant for simulation purposes.

Boitiaux et al. [2] quoted values of activation energy between 38,000 and 42,000 J/mol for the hydrogenation reactions of 1,3-butadiene and 1-butene (reactions 2–5) and isomerizations of the latter (reactions 8 and 9) on Pd-based catalysts. The values of apparent activation energy found for reactions 5, 8 and 9 are about half those values, suggesting that strong intra-particle effects take place on the tested catalyst.

Table 1
Kinetics expressions and kinetics parameters

$r_1 = k_1 x_{PE} x_{H_2}/(1 + \kappa_{ad} x_{un})$	
$r_2 = k_2 x_{BD} x_{H_2}/(1 + \kappa_{ad} x_{un})$	
$r_3 = k_3 x_{BD} x_{H_2}/(1 + \kappa_{ad} x_{un})$	
$r_4 = k_4 x_{BD} x_{H_2}/(1 + \kappa_{ad} x_{un})$	
$r_5 = k_5 x_{1BE} x_{H_2}/(1 + \kappa_{ad} x_{un})$	
$r_6 = k_6 x_{cBE} x_{H_2}/(1 + \kappa_{ad} x_{un})$	
$r_7 = k_7 x_{tBE} x_{H_2}/(1 + \kappa_{ad} x_{un})$	
$r_8 = k_8[x_{1BE} - x_{cBE}/K_8^e]$	
$r_9 = k_9[x_{1BE} - x_{tBE}/K_9^e]$	
$k_1 = 628.7$ mol/kg s	
$k_2 = 565.8$ mol/kg s	
$k_3 = 226.3$ mol/kg s	
$k_4 = 339.5$ mol/kg s	
$k_5 = 229.1$ mol/kg s	$E_5 = 21{,}793$ J/mol
$k_6 = 355.4$ mol/kg s	$E_6 = 10{,}832$ J/mol
$k_7 = 273.3$ mol/kg s	$E_7 = 13{,}140$ J/mol
$k_8 = 1.768 \times 10^{-1}$ mol/kg s	$E_8 = 18{,}751$ J/mol
$k_9 = 3.452 \times 10^{-1}$ mol/kg s	$E_9 = 18{,}965$ J/mol
$\kappa_{ad} = 75$	

3. Reactor model

In order to formulate a mathematical model for an industrial adiabatic hydrogenation reactor, a number of hypotheses related to fluid dynamics and transport properties [4,6,13] can be adopted once process conditions, namely bed geometry, operating variables and fluid properties, are established. A set of conditions is defined in Table 2. The composition of a typical C_3–C_4 refinery stream and reaction conditions similar to those employed in selective hydrogenation processes [1] for olefins reach cuts have been considered.

Properties pertaining to both fluid phases, vapour and liquid, are summarised in Appendix A. Details about how they were evaluated are given in [12].

The relevant hypotheses are:

(a) uniform flow distribution for both, vapour and liquid phases;
(b) the catalytic pores are filled up with liquid and the external particle surface is completely wetted;
(c) axial dispersion in both phases is ignored;
(d) phase-equilibrium at the bed inlet;
(e) thermal equilibrium between the fluid phases holds at a given axial position;
(f) H_2 transfer through the liquid film is the only rate-limited process regarding vapour–liquid mass exchange;
(g) mass transfer effects inside the catalyst particles and catalytic kinetics are lumped into effective reaction rate expressions (Table 1).

An analysis about these listed assumptions can be found in [12]. However, some remarks will be made about hypotheses (c) and (f), as they are specific to the conditions of the process studied.

Axial dispersion in the liquid phase of packed beds with two-phase up-flow is known to be significant [4–6]. Two correlations [14,15] have been employed to evaluate Pe_L (Peclet number based on particle diameter). The expression of Stiegel and Shah [14] has been chosen as it provides lower (conservative) values. Considering the ratio Z_L/d_{pe} given in Table 2, a value $Pe'_L = Pe_L(Z_L/d_{pe}) = 105$ is estimated. According to Lamine et al. [16], axial dispersion effects can be neglected when $Pe'_L > 100$. Therefore, this criterion provides a rationale for accepting hypothesis (c).

As regards to hypothesis (f), it should be first considered that H_2 will be transferred from the vapour to the liquid phase, due to the hydrogenation reactions, and hydrocarbons will normally move from the liquid to vapour, due to the temperature rise along the bed. On the liquid side of the interface, the resistance to H_2 transport should be considered, but hydrocarbons, as a whole, will not face any hindrance on the liquid side, as their overall mole fraction is nearly the unity.

To check if mass transfer limitations on the vapour side might be of certain significance, we can consider the following expression (Wesselingh and Krishna [17]) for the H_2 driving force in the vapour side:

$$\delta y = y_{H_2} - y^{i}_{H_2} = \frac{y_{HC} N^{VL}_{H_2} + y_{H_2}(-N^{VL}_{HC})}{k^{V}_{H_2}} \quad (2)$$

in which binary mass transfer coefficients between H_2 and each hydrocarbon species were assumed to have the same value, $k^{V}_{H_2}$. In Eq. (2) $y_{HC} = 1 - y_{H_2}$ is the mole fraction of the hydrocarbon lump. As $N^{VL}_{H_2}$ is controlled by the very low H_2 liquid solubility, it can be reasonably argued that this flux will not generate any concentration gradient on the vapour side. Instead, the magnitude of $(-N^{VL}_{HC})$ is not easily predictable. The results from the simulations assuming hypothesis (f) as being true can be used to estimate $(-N^{VL}_{HC})$ and $N^{VL}_{H_2}$ and y_{H_2}. Although values of $(-N^{VL}_{HC})$ up five times those of $N^{VL}_{H_2}$ arise, it was checked, by using Eq. (2), that δy remains safely below 1% of either y_{H_2} or y_{HC}. It can be concluded that no composition gradients are built within the vapour phase either for H_2 or for the hydrocarbon lump. The same conclusion also applies on the basis of individual hydrocarbon species.

Having taken into account hypotheses (a) to (g), the formulation of the model will be summarised next.

Table 2
Operating conditions for total hydrogenation

Inlet temperature (T^0)	313.16 K
Pressure (P)	1.2 MPa
Catalyst: 3-lobe particle (d_{pe})	0.00225 m
Reactor diameter (d_T)	0.58 m
Bed porosity	0.45
Molar flow (hydrocarbons)	26.60 mol/s
Molar flow (H_2)	0.67 mol/s
Reactor length (Z_L)	2.3 m
Compound	**Molar percentage**
Methane	0.6148
Ethane	3.824
Propane	21.76
Propene	0.4304
1,3-Butadiene	0.1697
1-Butene	0.7869
2-Butene (*cis* + *trans*)	0.0
n-Butane	14.30
i-Butane	58.11

3.1. Mass transfer steps

For H_2 on the liquid film at the vapour–liquid interface,

$$N^{VL}_{H_2} = k^{L}_{H_2} C^{L}_{T}(x^{i}_{H_2} - x_{H_2}) + N^{VL}_{T} x_{H_2} \quad (3)$$

The effect of the overall flux N^{VL}_{T} on the mass transfer coefficient was neglected, as small ratios $(N^{VL}_{T}/k^{L}_{H_2})$ hold in practice.

For the fluxes from the liquid bulk to the catalytic surface,

$$N^{LS}_{j} = k^{S}_{j} C^{L}_{T}(x_j - x^{S}_{j}) + N^{LS}_{T} x_j \cong k^{S}_{j} C^{L}_{T}(x_j - x^{S}_{j}); \quad \forall j \quad (4)$$

The approximation expressed by the last term in Eq. (4) arises from the fact that all reacting species are very diluted (including H_2) and, from stoichiometry, $N_T^{LS} = N_{H_2}^{LS}$.

3.2. Material balances

In order to evaluate the total molar flow of any component F_j at a given axial position, it is only necessary to write down differential conservation expressions for a number of key components that equals the number of linearly independent reactions. A set of five key components should be selected for the nine reactions considered in Fig. 2. The five unsaturated species (assumed to be indexed from $j = 1$ to 5) can be conveniently taken to this end. Then,

$$\frac{1}{A_f}\frac{dF_j}{dZ} = \rho_b r_j^S; \quad j = 1, \ldots, 5; \qquad F_j(0) = F_j^0 \tag{5}$$

where r_j^S is the net production rate for species j, expressed from the reaction network in Fig. 2, and the superscript "S" is used to remind that the reaction rates should be evaluated at molar fractions x_j^S. So, to evaluate r_j^S,

$$a_v^{LS} k_j^S C_T^L (x_j - x_j^S) = \rho_b r_j^S; \quad j = 1, \ldots, 5 \tag{6}$$

For the remaining species,

$$F_j = F_j^0 + \sum_{k=1}^{5} \alpha_{kj}(F_k - F_k^0); \quad j > 5 \tag{7}$$

where α_{kj} is the stoichiometric coefficient of a non-key species ($j > 5$) in the formation reaction of the key-species k ($1 < k < 5$).

An additional conservation equation for H_2 in the liquid phase is needed to account for its mass transfer limitations in the vapour–liquid interface,

$$\frac{1}{A_f}\frac{dL_{H_2}}{dZ} = a_v^{VL} N_{H_2}^{VL} - a_v^{LS} N_{H_2}^{LS}$$

Considering Eqs. (3) and (4), $L_{H_2} = x_{H_2} L$ and $dL/dZ = (a_v^{VL} A_f) N_T^{VL} - (a_v^{LS} A_f) N_T^{LS}$; then

$$\frac{L}{A_f}\frac{dx_{H_2}}{dZ} = a_v^{VL} k_{H_2}^L (x_{H_2}^i - x_{H_2}) - a_v^{LS} k_{H_2}^S (x_{H_2} - x_{H_2}^S) \tag{8}$$

To specify composition in both phases, x_j and y_j, we should consider the equilibrium relationships at the vapour–liquid interface, which accounting for the fact that H_2 is the only limited species can be written

$$y_j = K_j x_j; \quad j \equiv \text{hydrocarbon} \tag{9a}$$

$$y_{H_2} = K_{H_2} x_{H_2}^i \tag{9b}$$

The Rachford–Rice equation [18] becomes modified as

$$\frac{(1 - K_{H_2})[z_{H_2} - (1 - V/F_T)x_{H_2}]}{K_{H_2}(V/F_T)} + \sum_{j \equiv HC} \frac{(1 - K_j)z_j}{1 + (K_j - 1)(V/F_T)} = 1; \quad z_j = \frac{F_j}{F_T} \tag{10}$$

where F_T, L and V are the mixture, liquid and vapour molar flows, and $F_T = L + V$. Once the value of (V/F_T) closing Eq. (10) is found, $x_j = L_j/L$ and $y_j = V_j/V$ follow.

3.3. Energy balance

As the reactor is adiabatic and thermal equilibrium is assumed for the vapour–liquid mixture, the value of temperature at a given axial position can be expressed as

$$T = T^0 + \frac{Q_r + Q_V}{\mathbb{C}_P} \tag{11}$$

where:

$$Q_r = \sum_{k=1}^{5} (-\Delta H_k)_L^0 (F_k - F_k^0); \qquad Q_V = \sum_{j=1}^{NC} \lambda_j^0 (V_j - V_j^0);$$

$$\mathbb{C}_P = \sum_{j=1}^{NC} (c_{P,j}^L L_j + c_{P,j}^V V_j) \tag{12}$$

where ΔH_k is the heat of formation of species k, and λ_j is the heat of vaporisation of species j. Although the molar heat $c_{P,j}^L$ and $c_{P,j}^V$ should be strictly computed as average values between the bed inlet and the given position, constant values evaluated at the bed inlet do not introduce any significant inaccuracy.

3.4. Pressure drop

The variation of total pressure is computed from

$$\frac{dP}{dZ} = \Delta P_b - P_s; \quad P(0) = P^0 \tag{13}$$

ΔP_b represents the dynamic pressure drop and P_s accounts for hydrostatic variations. Expressions to evaluate both terms are given in Appendix A.

3.5. Numerical solution

The proposed model comprises seven ordinary first order differential equations (5, 8 and 13), six non-linear algebraic equations (6 and 10) and some linear relations. This system was solved by means of the code DDASAC [9].

4. Results: analysis and discussion

The set of operating conditions given in Table 2 has been taken as a base case to describe the behaviour of the hydrogenation process, according to the model discussed earlier. An outline of the main features will be first given later on. The effect of operating variables, temperature, pressure and H_2 input, will be discussed later. Finally, some considerations about the relative amounts of unsaturates in the process stream will be given. The values given in Table 2 will

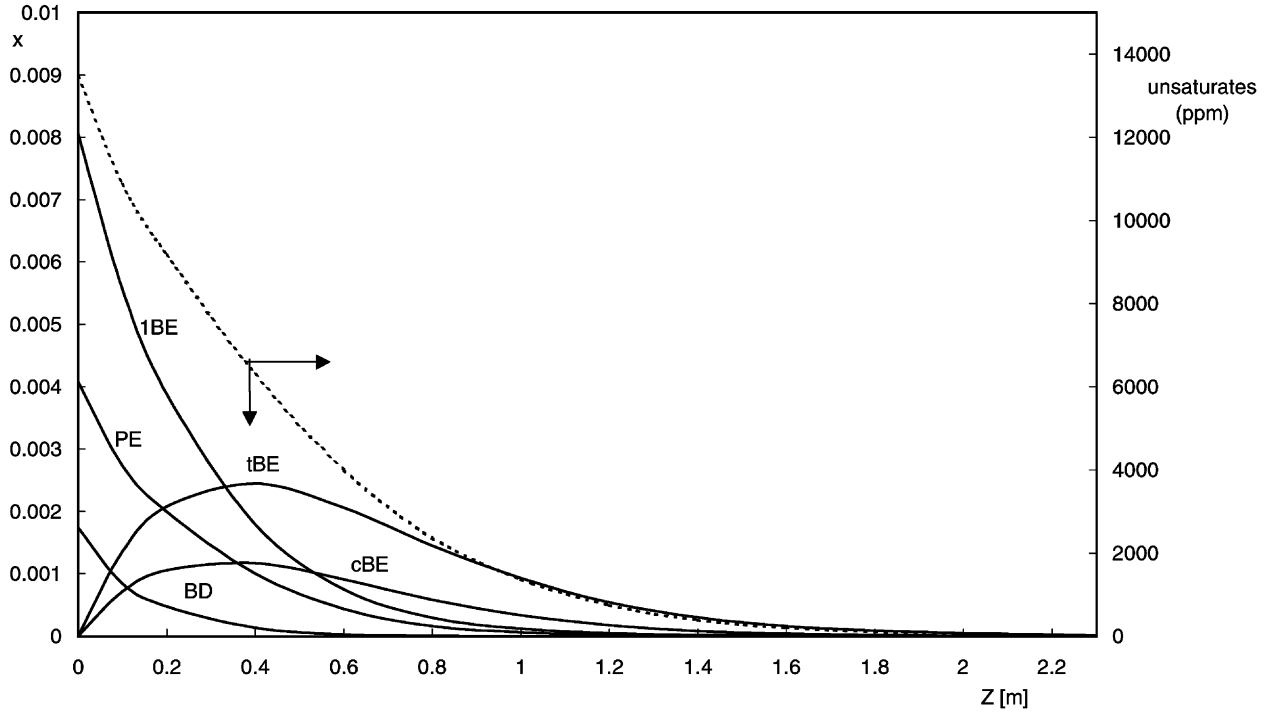

Fig. 3. Molar fraction profiles in liquid phase and total amount of unsaturates. Base case (Table 2). PE: propene; BD: 1,3-butadiene; 1BE: 1-butene; cBE: *cis*-2-butene; tBE: *trans*-2-butene.

be maintained in the remaining of this section, except when explicitly noted.

4.1. Overall behaviour

The evolution of the unsaturate liquid mole fractions along the catalytic bed is depicted in Fig. 3. The total amount of unsaturates, expressed in molar ppm, is also plotted in Fig. 3. The unsaturates content at the bed exit was fixed at 20 ppm. This is a realistic tolerance, which allowed defining the bed length in Table 2.

Propene and 1,3-butadiene are hydrogenated faster than 1-butene. This assertion is true, although the pattern followed by x_{1BE} in Fig. 3 is the result of 1-butene formation from 1,3-butadiene (reaction 2 in Fig. 2), hydrogenation to *n*-butane (reaction 5) and isomerization to 2-butenes (reactions 8 and 9).

Next in the hydrogenation rate ranking is *cis*-2-butene and, finally, *trans*-2-butene is the slowest species. It is recalled that both 2-butenes were not present in the specific stream considered in Table 2, but they are formed from 1,3-butadiene and 1-butene (reactions 3, 4, 8 and 9). It can be observed in Fig. 3 that the second half of the bed is almost exclusively needed to hydrogenate the 2-butenes, particularly *trans*-2-butene.

The fast hydrogenation of propene and 1,3-butadiene causes a sudden drop in the liquid mole fraction of H_2, as can be appreciated in Fig. 4. The comparison of x_{H_2} with the interface equilibrium value, $x^{i}_{H_2}$, in Fig. 4 clearly reveals that significant mass transfer limitations takes place at the vapour–liquid interface in the first part of the bed. After $Z = 0.2$ m, the consumption of H_2 is nearly equilibrated by mass transfer from the vapour phase and only in the last part of the bed, when the slow *trans*-2-butene hydrogenation is the only significant reaction taking place, the liquid stream nearly reaches saturation conditions.

On the other hand, mass transfer from the liquid to the catalytic surface turns out to be fast enough to keep $x^{S}_{H_2}$ close to x_{H_2} along the whole bed.

A quite significant decrease in the H_2 vapour mole fraction y_{H_2} can be observed in Fig. 4. This is partially due to the overall H_2 consumption, but the main reason is the temperature rise, which increases the volatility of the hydrocarbon mixture. The profiles of T, V_{HC} and V_{H_2} are plotted in Fig. 5. The heat released by the hydrogenation of each double bond of any of the unsaturated compounds is nearly the same, about 125,000 J/mol. Out of the total heat released, around 30% is employed to vaporise a fraction of the hydrocarbon mixture. Therefore, the temperature rise of the mixture is damped in the same proportion.

V_{HC} increases at the bed exit with 42% of the value at the inlet. Although this increment and its associated effects on temperature rise and on H_2 vapour molar fraction are important for the system behaviour, it only amounts to 2.5% of the overall hydrocarbon flow rate.

For the analysed base case, the outcome from variations of V_{HC} and V_{H_2} is a net increase in the total vapour molar flow (around 17% from bed inlet to outlet) that makes the

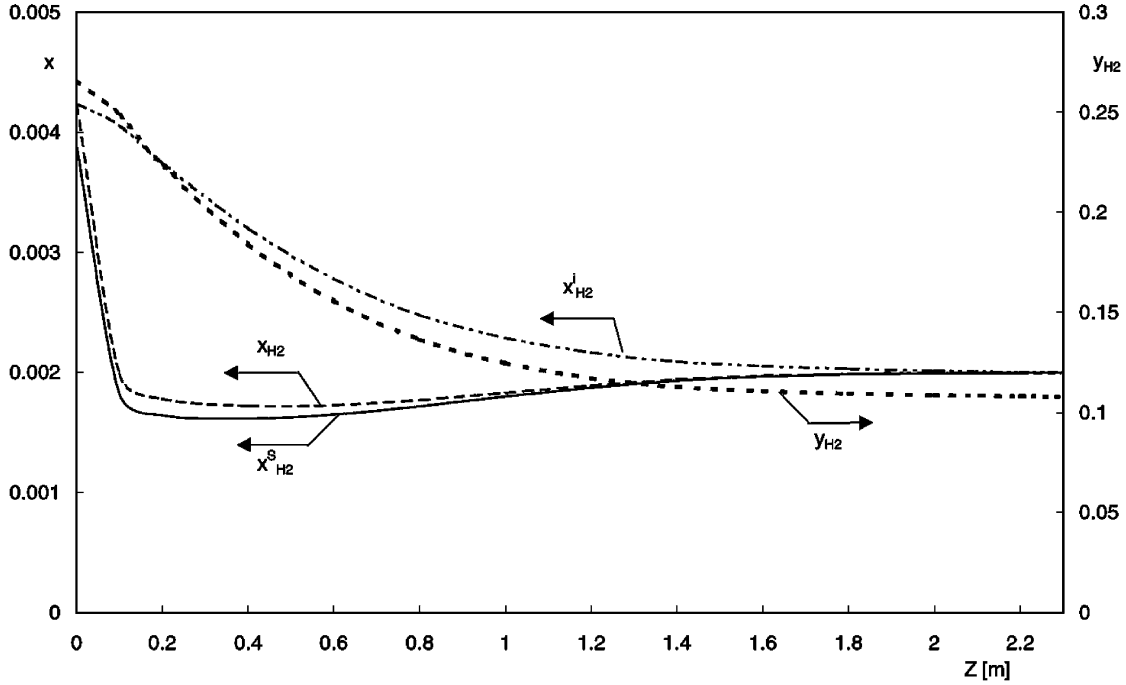

Fig. 4. Hydrogen molar fraction profiles. Base case (Table 2).

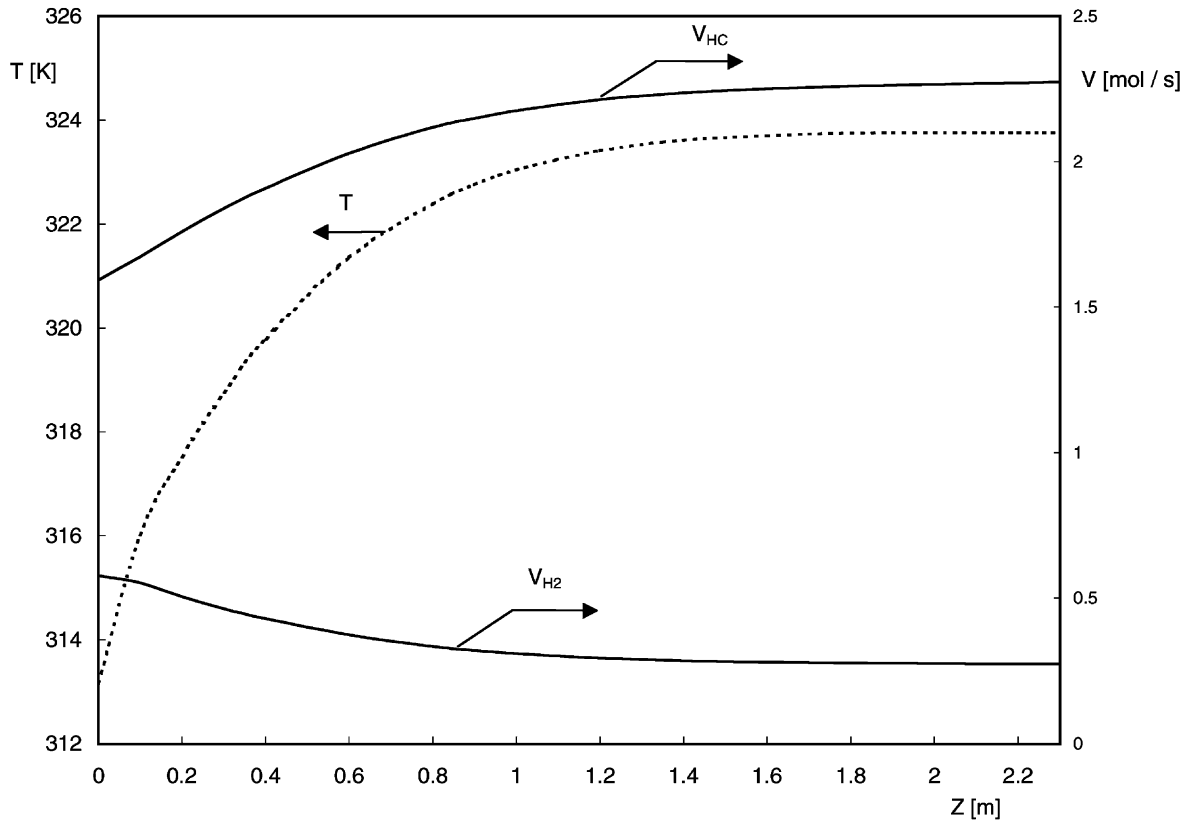

Fig. 5. Temperature, T; hydrogen vapour molar flow, V_{H_2}; and hydrocarbon vapour molar flow, V_{HC} profiles. Base case (Table 2).

Table 3
Effect of hydrogen flow rate on reactor performance

Case	F_{H_2} (mol/s)	F_{H_2}/F_{H_2}(st)	V^0 (mol/s)	ΔV (mol/s)	V^0_{HC} (mol/s)	ΔV_{HC} (mol/s)	$\Delta T = T^e - T^0$ (K)
a	0.627	1.78	2.04	0.32	1.50	0.63	10.86
b	0.667	1.90	2.17	0.38	1.59	0.68	10.61
c	1.253	3.56	3.94	0.81	2.78	1.13	8.41
d	1.880	5.35	5.69	1.04	3.90	1.36	7.19
e	2.507	7.13	7.34	1.18	4.92	1.51	6.39

specific mass transfer coefficient ($a_v^{VL}k_{H_2}^L$) rise 27%. This fact is of some significance, because of the H_2 transport limitations already commented on.

4.2. Effect of operating variables

4.2.1. H_2 input

The H_2 molar flow fed into the bed can be operatively increased from the stoichiometric value needed to hydrogenate the unsaturates. We will analyse here the impact of increasing $F^0_{H_2}$, focusing on the bed length required to achieve the goal of the process, i.e. as a means to reduce the catalyst loading or to compensate for activity losses. However, the final decision on the magnitude of $F^0_{H_2}$ should be taken on economic grounds, as bed pressure drop and H_2 recycling should also be considered.

Five levels of $F^0_{H_2}$ has been tested, ranging from a low value showing a ratio of 1.78 with respect to the stoichiometric value (Case (a) in Table 3) up to a four-fold value (Case (e)). Case (b) in Table 3 correspond to the base case.

It can be expected that increasing $F^0_{H_2}$ will, in some way, increase the H_2 concentration on the catalyst surface, $x^S_{H_2}$. The hydrogenation reactions (Table 1) will become faster and a shorter catalytic bed will be needed. Note that the isomerization reactions 8 and 9 are independent of $x^S_{H_2}$. Hence, they will not benefit from higher values of $x^S_{H_2}$ and lower amounts of 2-butenes will be produced from 1-butene, saving an important amount of catalyst otherwise needed to accomplish their slow hydrogenation.

It is shown in Fig. 6 that $x^S_{H_2}$ significantly increases as $F^0_{H_2}$ is raised, causing important reductions in bed length, which can be read at the point where each curve ends. By doubling $F^0_{H_2}$, i.e. from Cases (a) to (c), the bed length to obtain 20 ppm of unsaturates at the exit diminishes by 33%. A four-fold increase in $F^0_{H_2}$ saves half of the catalytic bed.

The increase in $x^S_{H_2}$ with $F^0_{H_2}$ is primarily caused by higher values of the H_2 vapour mole fraction y_{H_2} and, secondarily, by higher values of ($a_v^{VL}k_{H_2}^L$) derived from higher vapour flow rates (see Table 3).

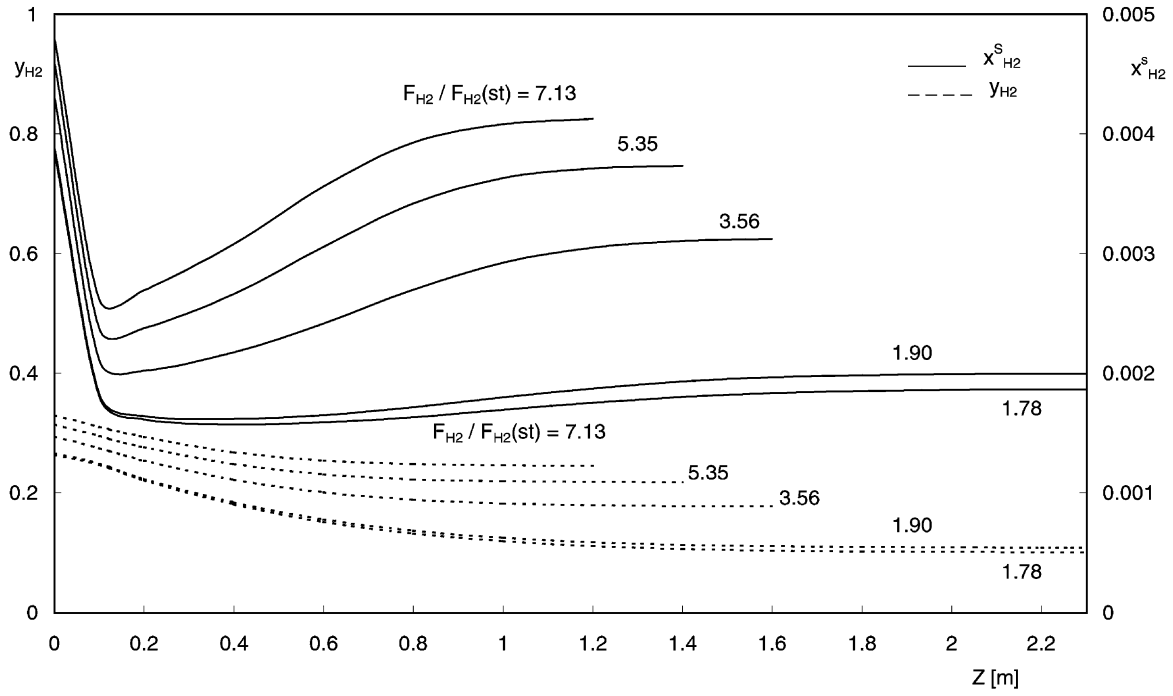

Fig. 6. Influence of H_2 molar flow on the calculated hydrogen molar fraction profiles.

In turn, the relative increase in the level of y_{H_2} (plotted in Fig. 6) arises from two sources. One of them is the direct effect caused from higher values of the overall fraction $z_{H_2} = F_{H_2}/F_T$. This can be appreciated at the bed inlet ($z = 0$) in Fig. 6, where T^0 is the same for all cases. It is clear that only relatively small differences arise. The second and main effect is due to the fact that larger amounts of HC can be vaporised along the bed as $F^0_{H_2}$ is raised (see Table 3). Thus, smaller temperature rises and, consequently, smaller y_{H_2} drops take place (see y_{H_2} profile in Fig. 6).

The values of temperature rise at the bed exit, ΔT, are given in Table 3. The different values of ΔT create another effect on their own: the kinetic coefficients increase in different degrees along the bed. In this regard, the increase of $F^0_{H_2}$ (ΔT is reduced) restrains a desirable side effect on catalyst saving, but the associated increase of $x^S_{H_2}$ is neatly overwhelming.

Summing up, $F^0_{H_2}$ will be relevant either as a design or as an operating variable. However, its effect is far from being obvious. If neither mass transfer limitations nor temperature variations along the bed had been taken into account, the effect of $F^0_{H_2}$ would have been hardly noticeable, as the effect of z_{H_2} at the inlet would have just remained. Going farther on this comparison, even this marginal difference would nearly disappear if only C_4 hydrocarbons were present (i.e. without C_2 and C_3 species), as all components would show similar volatilities and the H_2–HC mixture would behave as a pseudo-binary mixture presenting equilibrium phase composition independent of z_{H_2} at fixed values of T and P.

4.2.2. Operating pressure

The direct mean to increase the solubility of H_2 is to raise the operating pressure. The partial pressure of the HC mixture at temperature $T^0 = 313.16$ K (base case) is about $P_{HC} = 0.75$ MPa. The difference ($P - P_{HC}$) nearly equals the H_2 partial pressure P_{H_2}. An increment from the operating pressure in the base case $P = 1.2$ to 1.5 MPa causes an increment of around 100% in P_{H_2}. Consequently, the equilibrium value $x^i_{H_2}$ becomes higher in about the same proportion.

As the HC vaporisation is restrained at higher pressures, the mixture temperature along the bed gets higher at $P = 1.5$ MPa, but causes a lower drop in y_{H_2}. The changes from bed inlet to exit are $\Delta V_{HC} = 0.0774$ mol/s (1.5 MPa) versus 0.6807 mol/s (1.2 MPa); $\Delta T = 13.2$ K (1.5 MPa) versus 10.6 K (1.2 MPa); $y^e_{H_2}/y^0_{H_2} = 0.5093$ (1.5 MPa) versus 0.4051 (1.2 MPa).

The differences just outlined lead to values of $x^S_{H_2}$ around 100% higher at $P = 1.5$ MPa, which along with the marginal effect of temperature allows a saving of somewhat more than 50% in the bed length needed to achieve 20 ppm of unsaturates at the bed exit. The profiles of $x^S_{H_2}$ at 1.2 and 1.5 MPa are compared in Fig. 7. The curve ends mark the necessary bed lengths. The profiles of *trans*-2-butene mole fraction are also given, recalling that this is the last unsaturate to get extinguished.

From the discussed example, it can be concluded that a significant effect on catalyst loading or on catalyst time on service can be achieved by increasing pressure in the range 0–1 MPa above the specific value of P_{HC}. While

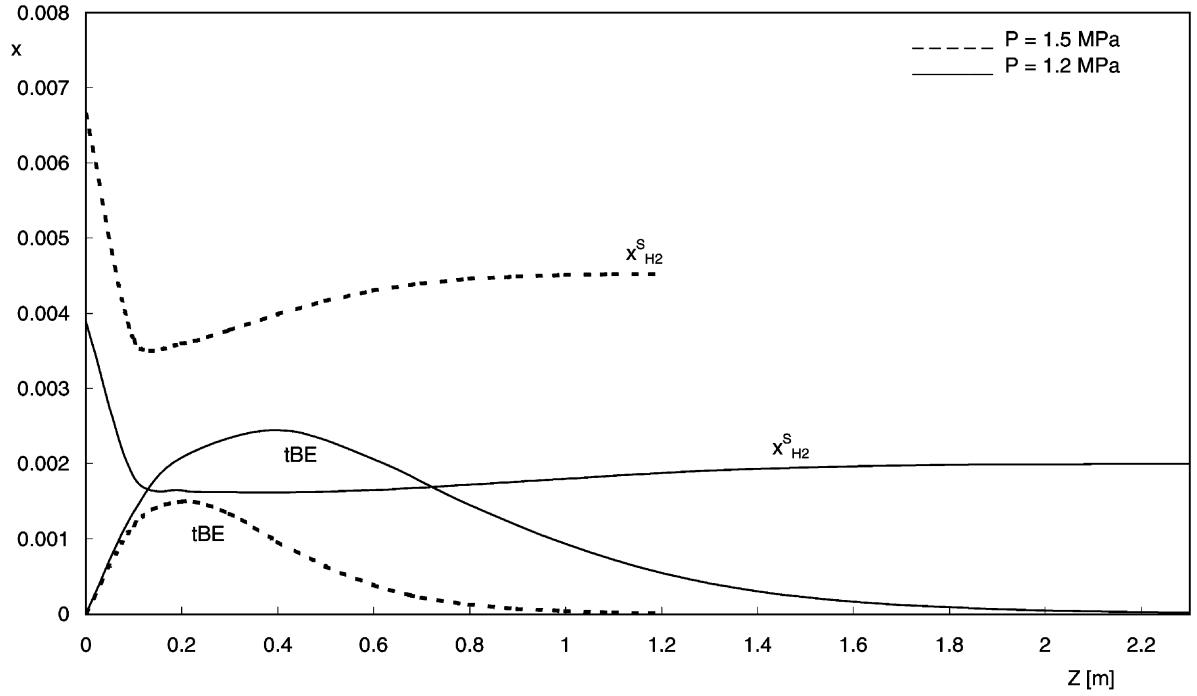

Fig. 7. Influence of the reactor pressure on calculated hydrogen molar fraction (at liquid–solid interphase), *trans*-2-butene molar fraction.

Table 4
Effect of inlet temperature on reactor performance

T^0 (K)	Outlet (ppm unsaturates)	ΔT (K)	V^0_{HC} (mol/s)	ΔV_{HC} (mol/s)
303.16	1.5	12.92	0.854	0.137
313.16	20	10.60	1.592	0.681
323.16	265	6.57	3.582	1.542

investment costs will not be greatly affected within this pressure range, the compression cost will naturally rise with P. Nonetheless, the possibility to increase reaction rates through P will become even more significant on the light of the results discussed next for the effect of operating temperature, the usual variable employed to modify reaction rates.

4.2.3. Inlet temperature

The conceptual arguments to assess the impact of increasing the thermal level of the mixture have been already discussed: on one hand, an increase in the HC volatility that will make y_{H_2} and consequently $x^S_{H_2}$ decrease and, on the other hand, an increase in the kinetic coefficients. As they show opposite effects on the hydrogenation rates, the net outcome should be quantitatively evaluated.

The results can be discussed from Table 4, where the inlet temperature was modified by ±10 K from the base-case value, $T^0 = 313.16$ K. The unsaturate concentration at the exit increases one order of magnitude for an increment of 10 K. The significant increase of V_{HC} as T^0 increases, not only at the bed inlet, but also along the bed (Table 4), causes a significant dilution of H_2 in the vapour phase that definitely overwhelms the effect on kinetic coefficients.

It becomes interesting to analyse whether catalysts with higher activation energies will still show the same trend with temperature. To this end, it was considered that at $T^0 = 313.16$ K, all hypothetical catalysts will show the same values of the kinetic parameters (those resulting for the material actually tested), but parameterized with an activation energy assumed common for all reactions. The concentration of unsaturates at the exit of a bed with $Z_L = 1.4$ m are plotted in Fig. 8 as a function of T^0 for different values of E. Values of T^0 above 293 K (20 °C) are considered, as it was appraised that sub-ambient temperatures will not be convenient. The results for the experimentally tested catalyst (Table 1) and for $E = 0$ are included. The latter is a limit case that just reflects the effect of T^0 on H_2 dilution in the vapour phase.

For any non-zero value of E, there is a lower range in which an increase of T^0 will be favourable to diminish the amount of unsaturates, but this trend is shifted after some value T^0_{crit} that increases with E.

The value T^0_{crit} for the tested catalyst is low (around 290 K), due to low effective activation energies. It can appreciated in Fig. 8 that the overall behaviour above T^0_{crit} does not differ much from the hypothetical case with $E = 0$. Most probably, this catalyst is subjected to significant internal diffusion limitations; therefore, the intrinsic activation energies could be of the order of 30,000–40,000 J/mol [2]. Thus, the curve for $E = 41{,}800$ J/mol in Fig. 8 may represent the behaviour of a catalyst without diffusion

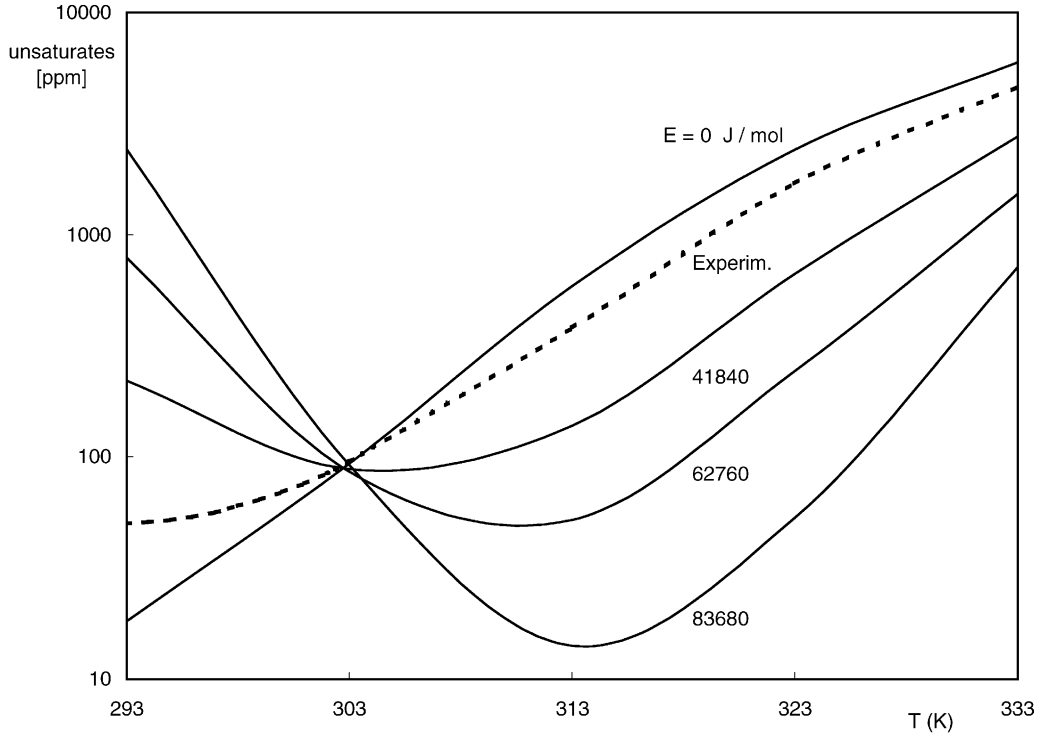

Fig. 8. Effect of the feed temperature on reactor behaviour. Five activation energy levels.

Table 5
Effect of percentage unsaturates inlet on the reactor performance

Case	Unsaturates at reactor inlet (ppm)			Unsaturates at reactor outlet ($Z_L = 2.3$ m) (ppm)			
	PE	BD	1BE	Total	PE	1BE	tBE
Base	4303.5	1696.8	7869.2	18.35	0.0	0.5	15.8
I	10295.1	0.0	3574.4	3.25	0.0	0.086	2.84
II	10295.1	1787.78	1787.78	8.2532	0.04	0.21	7.03
III	10295.1	3574.4	0.0	21.17	0.17	0.53	17.36
IV	2058.28	0.0	11809.91	10.30	0.0	0.27	9.025
V	2058.28	5904.34	5904.34	151.35	0.17	3.65	122.27
VI	2058.28	11809.91	0.0	1466.7	13.56	34.88	1047.28

limitations. T^0_{crit} rises to 303 K, but the range of T^0 producing a favourable effect is still limited.

The other values of E, although improbable for Pd-based catalysts, are helpful to visualise that the effect of temperature may change, depending on the specific system being analysed. Other modifications leading to reduce the HC volatility will also make T^0_{crit} increase, e.g. higher pressures or lower concentration of C_3 species.

Summing up, the effect of temperature will be uncertain without a quantitative analysis. At the realistic conditions here studied, increasing operating temperature turns out to be definitely detrimental, leaving variables such as $F^0_{H_2}$ or P as a mean to improve the performance of the unit.

4.2.4. Unsaturate composition

We intend to show here that the design of the purification unit and/or its operating policy will be strongly affected by the composition of the stream to be purified. To this end, we will consider the base case defined in Table 2 and evaluate how the unsaturate content at the exit is changed by modifying the participation of each unsaturate in the hydrocarbon stream, while leaving fixed the overall unsaturate concentration.

The results for different combinations are displayed in Table 5. Cases I–III show a high propene level and Cases IV–VI a low propene level. Within each group, the relative amounts of 1,3-butadiene and 1-butene were modified at the expense of each other. It can be first noted that the overall amount of unsaturates at the exit varies within almost three order of magnitudes, revealing quite significant differences in the behaviour of the three unsaturates.

It can be appreciated in Table 5 that propene is the most desirable species out of the three. This is due to its relatively high hydrogenation rate and the fact that just one saturated compound (propane) is formed. On the other hand, 1,3-butadiene is the worst. The primary reason for this conclusion is that the relatively slow reacting *n*-butenes are the intermediate products from 1,3-butadiene hydrogenation. In addition, 1,3-butadiene releases nearly twice the heat the olefins do, once hydrogenation is completed; hence, as the base case is unfavourably affected by temperature rises, the relative increase in 1,3-butadiene input impairs the process performance.

The case when the inlet concentration of any unsaturate increases independently will not be treated here, as it obviously will produce a rise in the overall unsaturate concentration at the bed outlet, if the remaining variables are left unchanged.

5. Conclusions

An analysis of operating conditions to hydrogenate unsaturate traces in C_3–C_4 streams, intended for aerosol propellant use, has been carried out. The behaviour of a three-phase fixed-bed catalytic unit operated in up-flow mode has been specifically undertaken.

Experiments on an "egg-shell" Pd-based commercial-catalyst have been conducted with the purpose of evaluating the main kinetic features. A simple scheme of the reactions taking place has been identified and effective kinetic expressions have been proposed to interpret quantitatively the experimental data. The hydrogenation rates of propene, of each *n*-butene (1-butene, *cis*-2-butene, *trans*-2-butene) and 1,3-butadiene (discriminating the relative amounts of each *n*-butene formed) could be evaluated, along with 1-butene isomerization rates. The relevant results were: *trans*-2-butene presents the slowest hydrogenation rate followed by *cis*-2-butene; the hydrogenation rates show a relatively high dependence with dissolved H_2 concentration, while the isomerization reactions show a weak dependence. The available data could be reasonably regressed with first and zero orders, respectively.

A mathematical model was proposed to describe the performance of a realistic industrial unit operated adiabatically. The model employs the results from the experimental kinetic study. Fluid dynamics, mass transfer limitations and phase-equilibrium were considered in the simplest possible way, but trying to avoid the loss of significant effects.

This model was then employed to simulate the operation of an industrial unit with the aim of identifying the most relevant features and evaluating the impact of operating variables on the performance of the unit.

Significant and non-obvious general features were:

- The slow hydrogenation of 2-butenes, specially of *trans*-2-butene, demands around half of the bed length.

2-Butenes can be present in the process stream, but they are always formed by hydrogenation of 1,3-butadiene and by isomerization of 1-butene.
- Mass transfer limitations on the liquid side of the vapour–liquid interface were most significant for H_2 absorption rates.
- The volatility of the hydrocarbon mixture was a paramount factor to dilute H_2 in the vapour phase (hence, to diminish the amount of H_2 dissolved in the liquid stream) and to restrain the temperature rise along the bed, due to the vaporisation heat.

These key factors allowed explaining the simulated response of the system to variations in the different operating variables. However, the results could be hardly predicted beforehand, due to the rather complex interplay of the effects. Thus, a temperature rise turned out to be significantly detrimental for the reactor performance at the conditions studied, as the effect of the increased hydrocarbon volatility overcomes the effect on the kinetic coefficients. A parametric analysis revealed that this result is not fortuitous and will stand for different catalysts and operating conditions.

The conclusion regarding the effect of temperature precludes the usual operating policy of rising temperature to compensate for catalytic activity decay. Instead, increasing the H_2 input and/or the operating pressure were shown to be effective alternatives to improve the reactor performance.

The reactor performance was also shown to be sensitive to the composition of the unsaturate pool, as the different compounds present significant differences concerning kinetics, reaction paths and thermal effects.

Acknowledgements

The financial assistance of ANPCyT (PICT 14-06297, P.BID 1201/OC-AR), CONICET (PIP96 4791) and UNLP (PI 1078) is acknowledged. J.A.A., N.J.M., O.M.M. and G.F.B. are members of CONICET, S.P.B. is member of CIC PBA.

Appendix A

Liquid and vapour properties evaluated at phase-equilibrium for conditions given in Table 2 are listed here, along with the source references.

Thermodynamic properties $c^{L}_{P,j}$, $c^{V}_{P,j}$, λ_j and $(-\Delta H_k)$ were evaluated from values reported in [21].

In simulating reactor performance, fluid properties and parameters (defined as follows) were updated along the bed, as the solution of the model equations proceeded.

Correlations employed to estimate hydrodynamic and transport parameters were:

- *Axial Peclet number*
  (a) Stiegel and Shah [14]

$$Pe_L = \frac{u_L d_{ps}}{D_{ax}} = \varepsilon_L 0.128\,\mathrm{Re}_{LS}^{0.245}\,\mathrm{Re}_{VS}^{-0.16}\left[\frac{a_v^{LS}}{(1-\varepsilon)}d_{ps}\right]^{0.53}$$

with

$$\mathrm{Re}_{Ls} = \frac{u_L \rho_L d_{ps}}{\mu_L}; \quad \mathrm{Re}_{Vs} = \frac{u_V \rho_V d_{ps}}{\mu_V}$$

To use this expression ε_L was evaluated from the expressions provided by the same authors [14]

  (b) Cassanello et al. [15]

$$Pe_L = 0.026(\mathrm{Re}_L \xi_{VL})^{0.302}$$

with

$$\xi_{VL} = \frac{1}{\varepsilon}(u_L + u_V)\,\Delta P_b + \frac{(u_L \rho_L + u_V \rho_V)}{\varepsilon} g$$

- *Pressure drop*
  (a) *Dynamic pressure drop*: Turpin and Hungtinton [22]

$$\Delta P_b = \frac{2 f_{VL} u_V^2 \rho_V}{d_h}$$

where

$$\ln f_{VL} = 8 - 1.12 \ln\omega - 0.079 \ln^2\omega + 0.0152 \ln^3\omega;$$
$$\omega = \frac{\mathrm{Re}_V^{1.167}}{\mathrm{Re}_L^{0.767}}$$

  (b) *Hydrostatic variation*

$$P_S = 9.81\left[\frac{\varepsilon_L}{\varepsilon}\rho_L + \frac{1-\varepsilon_L}{\varepsilon}\rho_V\right]$$

  (c) *Mass transfer coefficient from liquid to particle surface*: Mochizuki [23]

$MW_L = 53{,}875\,kg/mol$		$MW_V = 35{,}569\,kg/mol$	
$\rho_L = 485.705\,kg/m^3$	[19]	$\rho_V = 35.569\,kg/m^3$	[19]
$\mu_L = 1.312 \times 10^{-4}\,kg/m\,s$	[19]	$\mu_V = 1.107 \times 10^{-5}\,kg/m\,s$	[19]
$D^L_{H_2-HC} = 3.544 \times 10^{-8}\,m^2/s$	[20]	$D^V_{H_2-HC} = 4.462 \times 10^{-6}\,m^2/s$	[19]
$D^L_{HC-HC} = 8.232 \times 10^{-9}\,m^2/s$	[19]	$D^V_{HC-HC} = 5.638 \times 10^{-7}\,m^2/s$	[19]
$\sigma = 5.384 \times 10^{-3}\,N/m$	[19]		

$$\frac{k_j^{\mathrm{S}} d_{\mathrm{h}}}{D_j^{\mathrm{L}}} = \begin{cases} (Sc_j^{\mathrm{L}})^{1/3}(1000 d_{\mathrm{ps}} - 2.2); & \mathrm{Re_{Lm}} < \mathrm{Re_c} \\ 550(Sc_j^{\mathrm{L}})^{1/3}\mathrm{Re}_{\mathrm{Lm}}^{0.14} d_{\mathrm{ps}}; & \mathrm{Re_c} < \mathrm{Re_{Lm}} < \mathrm{Re_s} \\ 0.75(Sc_j^{\mathrm{L}})^{1/3}\mathrm{Re}_{\mathrm{Lm}}^{0.5}; & \mathrm{Re_{Lm}} > \mathrm{Re_s} \end{cases}$$

where

$$\mathrm{Re_{Lm}} = \frac{u_{\mathrm{L}} \rho_{\mathrm{L}} d_{\mathrm{h}}}{\mu_{\mathrm{L}}}; \quad Re_{\mathrm{c}} = 0.312 \exp(341 d_{\mathrm{ps}}); \quad Re_{\mathrm{s}} = 7.77 \exp(334 d_{\mathrm{ps}}); \quad d_{\mathrm{ps}}[=]\mathrm{m}$$

(d) *Mass transfer coefficient from vapour–liquid interface to liquid bulk*: Lara Márquez [24]

$$k_j^{\mathrm{L}} a_v^{\mathrm{VL}} = 40 (D_j^{\mathrm{L}})^{0.5} \xi_{\mathrm{VL}}^{0.5};$$

$$a_v^{\mathrm{VL}} = 2.36 \frac{(1 - \varepsilon_{\mathrm{L}}/\varepsilon)\rho_{\mathrm{L}}^{0.2} \xi_{\mathrm{VL}}^{0.4}}{\sigma^{0.6}}$$

ξ_{VL}: same parameter defined in Cassanello et al. [15].

(e) *Mass transfer coefficient from vapour bulk to vapour–liquid interface (inside bubbles)*: Wesselingh and Krishna [17]

For “mobile interfaces”,

$$k_j^{\mathrm{V}} = \frac{0.4}{[1 + (\rho_{\mathrm{V}}/\rho_{\mathrm{L}})^{1/2}]^{1/2}} \left[\frac{g^2 (\rho_{\mathrm{L}} - \rho_{\mathrm{V}})^2}{\mu_{\mathrm{L}} \rho_{\mathrm{L}}} (D_j^{\mathrm{V}})^3 \right]^{1/6}$$

(f) *Liquid hold-up*: Yang et al. [25]

$$\varepsilon_{\mathrm{L}} = \varepsilon - 0.28 \frac{u_{\mathrm{V}}}{u_{\mathrm{L}} + u_{\mathrm{V}}}$$

References

[1] M.L. Derrien, Selective hydrogenation applied to the refining of petrochemical raw materials produced by steam cracking, in: Stud. Surf. Sci. Catal. 27, L. Cerveny (Ed.), Catalytic Hydrogenation, Elsevier, 1986 (Chapter 18).

[2] J.P. Boitiaux, J. Cosyns, M. Derrien, G. Leger, Proper design of butadiene selective hydrogenation process for maximum 1-butene yield by using comprehensive kinetic modelling, AIChE Spring National Meeting, Houston, 1985.

[3] C.A. Vergel Hernández, Les réacteurs catalytiques a lit fixe avec ecoulement de gaz et de liquide, Comparaison sur le plan theorique et experimental de la performance du reacteur dans differents sens d’ecoulement, These de Docteur de l’Institut National Polytechnique de Lorraine, France, 1993.

[4] U. Herrmann, G. Emig, Liquid phase hydrogenation of maleic anhydride to 1,4-butanediol in a packed bubble column reactor, Ind. Eng. Chem. Res. 37 (1998) 759–769.

[5] C. Julcour, F. Stüber, J.M. Le Lann, A.M. Wilhelm, H. Delmas, Dynamics of three-phase up-flow fixed-bed catalytic reactor, Chem. Eng. Sci. 54 (1999) 2391–2400.

[6] K.B. Van Gelder, P.C. Borman, R.E. Weenik, K.R. Westerterp, Three-phase packed bed reactor with an evaporating solvent. II. Modelling of the reactor, Chem. Eng. Sci. 45 (1990) 3171–3192.

[7] N.O. Ardiaca, S.P. Bressa, J.A. Alves, O.M. Martínez, G.F. Barreto, Experimental procedure for kinetic studies on egg-shell catalysts: the case of liquid-phase hydrogenation of 1,3-butadiene and *n*-butenes on commercial Pd catalysts, Catal. Today 64 (2001) 205–215.

[8] S.P. Bressa, Purificación catalítica de 1-Buteno: estudio cinético y simulación de un reactor industrial de hidrogenación selectiva, Tesis Doctoral, U.N.L.P., 2001.

[9] W.E. Stewart, M. Caracotsios, J.P. Sørensen, Parameter estimation from multiresponse data, AIChE J. 38 (1992) 641–650.

[10] S. Dahl, S. Fredenslund, P. Rasmussen, The MHV2 model: a UNIFAC-based equation of state model for prediction of gas solubility and vapour–liquid equilibria at low and high pressure, Ind. Eng. Chem. Res. 30 (1991) 1936–1945.

[11] B. Larsen, P. Rasmussen, A. Fredenslund, A modified UNIFAC group-contribution model for prediction of phase equilibria and heats of mixing, Ind. Eng. Chem. Res. 26 (1987) 2274–2286.

[12] N.O. Ardiaca, S.P.Bressa, J.A.Alves, O.M. Martínez, G.F. Barreto, Selección de catalizadores y determinación de parámetros cinéticos para el diseño de un reactor de hidrogenación total de olefinas y di-olefinas de una corriente C_3–C_4, Internal Report, 1996.

[13] C. Krishnan, J.R. Elliot Jr., J.M. Berty, Simulation of a three-phase reactor for the solvent methanol process, Chem. Eng. Commun. 105 (1991) 155–170.

[14] G.J. Stiegel, Y.T. Shah, Backmixing and liquid hold-up in a gas–liquid concurrent up-flow packed column, Ind. Eng. Chem. Proc. Des. Dev. 16 (1977) 37–43.

[15] M.C. Cassanello, O.M. Martínez, A.L. Cukierman, Liquid hold-up and backmixing in concurrent up-flow three-phase fixed-bed reactor, Chem. Eng. Sci. 53 (1998) 1015–1025.

[16] A.S. Lamine, M.T. Colli Serrano, G. Wild, Hydrodynamics and heat transfer in packed bed with concurrent up-flow, Chem. Eng. Sci. 47 (1992) 3493–3500.

[17] J.A. Wesselingh, R. Krishna, Mass Transfer in Multicomponent Mixtures, Delft University Press, Delft, 2000.

[18] D.W. Green, J.O. Maloney, Perry’s Chemical Engineers’ Handbook, 7th Edition, McGraw-Hill, New York, 1997.

[19] R.C. Reid, J.M. Prausnitz, B.E. Poling, Properties of Gases and Liquids, 4th Edition, McGraw-Hill, New York, 1987.

[20] A. Akgerman, J.L. Gainer, Diffusion of gases in liquids, Ind. Eng. Chem. Fundam. 11 (1972) 373–378.

[21] T.E. Daubert, R.P. Danner, Physical and Thermodynamic Properties of Pure Chemicals, Data Compilation, Taylor & Francis, London, 1994.

[22] J.L. Turpin, R.L. Hungtinton, Prediction of pressure drop for two-phase, two-component concurrent flow in packed beds, AIChE J. 13 (1967) 1196–1202.

[23] S. Mochizuki, Empirical expressions of liquid–solid mass transfer in concurrent gas–liquid up-flow fixed-beds, Chem. Eng. Sci. 37 (1982) 1422–1424.

[24] A. Lara Márquez, Les réacteurs a lit fixe à co-courant vers le haut de gaz et de liquide, Etude de transfert de matière gaz-liquide, These de Docteur de l’Institut National Polytechnique de Lorraine, France, 1992.

[25] X.L. Yang, J.P. Euzen, G. Wild, Etude de la rétention liquide dans les réacteurs à lit fixe avec écoulement à cocourant ascendent de gaz et de liquide, Entropie 150 (1989) 17–28.